Observation of optical second-harmonic generation in porous-silicon-based photonic crystals in the Laue diffraction scheme

D. A. Kopylov,* S. E. Svyakhovskiy, L. V. Dergacheva, V. A. Bushuev, B. I. Mantsyzov, and T. V. Murzina
Physics Department, Moscow State University, 119991 GSP-1, Leninskie Gory, Moscow, Russia
(Received 31 December 2015; published 31 May 2016)

Second-harmonic generation (SHG) in the Laue scheme of the dynamical Bragg diffraction in one-dimensional photonic crystal (PhC) is studied. The experiments are performed for partially annealed porous-silicon PhC containing 250 periods of the structure. Our measurements confirm that the phase-matched optical SHG is observed under the Bragg conditions, which is evidenced by a narrow angular and spectral distribution of the diffracted SHG outgoing the PhC. This is confirmed by both the analytical description of the SHG process performed in the two-wave approximation, and by direct calculations of the PhC dispersion curves for the fundamental and SHG wavelengths by the revised plane wave method. Possible types of phase- and quasi-phase-matching realized in the studied PhC under the Laue diffraction scheme are discussed.

DOI: 10.1103/PhysRevA.93.053840

I. INTRODUCTION

Nonlinear optical effects in spatially periodic dielectric structures, referred to now as photonic crystals (PhCs), have been intensively studied over recent decades. Unlike conventional anisotropic nonlinear crystals, which are commonly used for an efficient frequency up-conversion, the PhCs are characterized by structural lattice-induced dispersion that gives additional possibilities for the realization of the phase-matching conditions for optical harmonics' generation. Their unique nonlinear-optical properties were first discussed in Ref. [1], where the quasi-phase-matching conditions for second-harmonic generation (SHG) in PhC were suggested involving necessarily the reciprocal lattice vector of a periodic medium [2–5]. Near the photonic band gap edge, phase-matching conditions can be satisfied due to an essential change of the effective refraction index of the composite media [6,7]. The efficiency of the SHG process is further enhanced by the spatial light localization in a PhC [8–10].

Similarly to x-ray diffraction in conventional electronic crystals, there are two main experimental geometries for the interaction of optical fields with PhCs, the so-called Bragg and Laue schemes. They differ by the way the light propagates inside the structure under the fulfillment of the Bragg diffraction condition. In the Laue transmission scheme in one-dimensional (1D) PhC, the light beam propagates parallel to the PhC layers. In that case, optical effects are described by the dynamical Bragg diffraction theory [11–15], where an interaction of so-called Borrmann (B) and anti-Borrmann (aB) modes existing in a PhC under the Bragg diffraction condition takes place. Being spatially localized in different types of PhC layers, they reveal different dispersion properties, which brings a number of specific effects. Among them, temporal Bragg-diffraction-induced laser-pulse splitting [12,13,16], pendulum effect [17–20] and selective compression of femtosecond laser pulses in 1D photonic crystals [14,21] were studied theoretically and experimentally. Importantly, contrary to the case of the Bragg (reflection) scheme, the photonic band gap is not formed in the Laue geometry, so that the radiation propagates without any exponential attenuation within a PhC. Thus the SH intensity could increase along all the length of the nonlinear structure participating in the SHG process in the Laue geometry.

An experimental realization of optical effects in the Laue diffraction geometry requires a high structural quality and relatively large sizes of the PhC cross section, or a large number of layers constituting a PhC. Thus, a flexible method for the PhC fabrication is needed, and a good candidate here is the electrochemical etching technique, which allows us to make porous-silicon-based PhCs with the number of layers up to several hundreds [22]. It provides acceptably large PhC geometrical sizes, a desired high modulation of the refractive indexes of the adjacent layers, etc. Importantly, such PhC reveals second- and third-order nonlinear properties as well, which were demonstrated up to now in the Bragg diffraction geometry [23–26], while in the Laue diffraction scheme these effects are much less studied. Theoretical aspects of SHG in the Laue geometry were first described in Ref. [27] and later in Ref. [28]. It was shown that different types of phase-matching conditions can contribute to the optical SHG process under the dynamical Bragg diffraction in the Laue geometry, which involves different combinations of the wave vectors of Borrmann and anti-Borrmann modes at both the fundamental and second-harmonic (SH) wavelengths. The first experimental evidence for SHG at hard x-ray wavelengths was reported recently in Ref. [29]. At the same time, to the best of our knowledge, there have been no experimental verifications of these ideas in optical PhCs.

In this paper we present the observation of phase-matched optical SHG in 1D partially annealed porous-silicon-based PhC in the Laue diffraction scheme. We demonstrate that two strong SHG peaks corresponding to the transmitted and diffracted fundamental beams obtained in the Laue scheme of diffraction are formed, which are associated with the phase-matched SHG effect. An additional type of quasi-phase-matched SHG appears as a less intensive intermediate SHG peak. The experimental observations are supported by the theoretical description of these phenomena. The paper is organized as follows: In Sec. II the methods of experiment and sample preparation are described. In Sec. III experimental results on the SHG in the Laue geometry are presented. Experimental

*kopylov.denis@physics.msu.ru

determination of the refractive indexes of the two types of PhC layers are described in Sec. IV. A theoretical description of SHG is presented in Sec. V, followed by discussion and conclusions. In the Appendix the experimental method of refractive indexes determination based on diffraction induced pulse splitting effect is described in detail.

II. EXPERIMENT

The samples under study are 1D photonic crystals based on mesoporous silicon multilayer structure made by electrochemical etching technique described in detail elsewhere [22]. In brief, a p-type crystalline silicon wafer of (100) crystallographic orientation and the resistivity of 0.005 Ω cm was used as a PhC template. The 1D porous-silicon-based PhC was formed by a periodic in time modulation of the electrochemical anodic current density j, the layers with low and high porosity were formed when using the values $j_1 = 40\text{mA/cm}^2$ and $j_2 = 100\text{mA/cm}^2$, respectively. Hydrofluoric acid of the mass concentration 28% was used as an electrolyte. The fabricated porous-silicon-based PhC consisted of 500 layers (250 periods of the PhC structure), each of them being 400 nm thick.

In order to increase the transparency of the porous-silicon-based PhC it was annealed at the temperature of 750 °C for five hours, so that an oxidation of the major part of crystalline silicon and formation of SiO_2 was attained. As a result, the PhC sample consisted of Si, SiO_2, and air, and the parameters of the constituting layers differ from those of the initial porous-silicon sample. Due to a volume expansion, the thickness of the layers in annealed PhC was approximately 440 nm. It is necessary to note that we definitely avoided the total oxidation of the PhC in order to keep a certain amount of crystalline silicon in the structure, which formed the second-order susceptibility on the Si-SiO_2 interfaces. After annealing the sample was cleaved into a rectangular block of the length $L = 500\mu$m.

For the experimental studies of SHG we used a setup based on a Ti:sapphire laser (with the wavelength of 800 nm, pulse duration of 100 fs, repetition rate of 80 MHz, the average power of 100 mW). The fundamental radiation was focused on the sample's facet by a 5 cm lens into a spot of approximately 50 μm in diameter, as is shown schematically in Fig. 1. The angle of incidence was close to the Bragg angle of the composed PhC, $\theta_B = 27^\circ \pm 0.25^\circ$. The SH radiation generated in transmission through the sample was gathered by a lens ($f = 5$ cm), passed through a diaphragm with $\oslash \approx 5$ mm, spectrally selected by a necessary set of filters (SCHOTT BG-39, Thorlabs FB400-10) and detected by a photomultiplier (Hamamatsu R4220P) operating in the photon-counting mode. In order to study the SHG diffraction, the PhC was placed on a rotation stage, so that the detection angle φ could be changed in the interval $[-40^\circ, +40^\circ]$ with an accuracy of 0.5°. Linear diffraction measurements were performed on the same setup where the blue filters were removed, and the photomultiplier was replaced by a Si-based photodiode.

Schematically, the experimental geometry along with the coordinate frame is shown in Fig. 1. The layers of different porosity are depicted by yellow and green colors, and the two directions that correspond to the transmitted (T) and diffracted (D) beams leaving the PhC are shown by red lines. The left-hand inset presents the orientation of pores with respect to the PhC facet. The p polarization of the fundamental electric field $E(\omega)$ lies in the (XOZ) plane and thus contains the projection of the electric field on the pores' axis as well as that perpendicular to them, while the s polarization of $E(\omega)$ is parallel to the (OY) axis and is perpendicular to the pores.

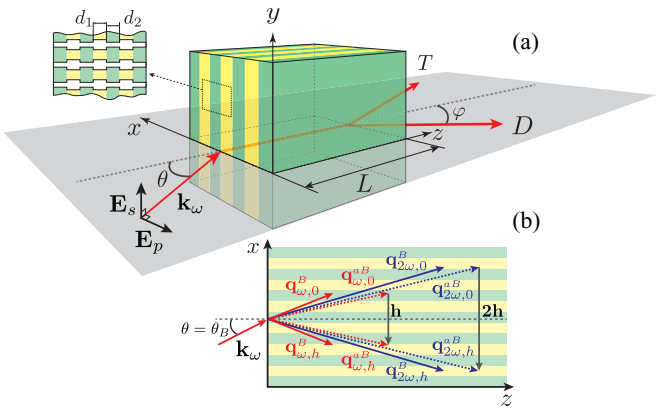

FIG. 1. (a) Schematic view of the dynamical diffraction of light in 1D PhC in the Laue geometry. Inset: the scheme of porous PhC microstructure with the layers of the thicknesses of d_1 and d_2. (b) Borrmann (B) and anti-Borrmann (aB) eigenvectors of the PhC for the fundamental (red) and SH (blue) waves, **h** stands for the reciprocal lattice vector. Diffracted (D) and transmitted (T) propagation directions of light are shown.

III. SECOND-HARMONIC GENERATION IN PHOTONIC CRYSTALS IN THE LAUE GEOMETRY

Figure 2(a) shows the SHG diffraction pattern obtained for the angle of incidence of the p-polarized fundamental beam $\theta = \theta_B$. For the comparison, the linear scattering indicatrix is shown as well. In both cases one can see two strong angular maxima, their angular positions correspond to the T and D directions and are centered at $\varphi = \pm 27^\circ$. Spectra of the registered signal revealed a narrow peak corresponding to the SHG wavelength, and its intensity was found to reveal a second-order dependence on the fundamental power, as is shown at the inset of Fig. 2(b). These data confirm that it was SH registered in the experiment. Importantly, the angular width of the SHG maxima is nearly twice smaller as compared to the linear diffraction peaks; the FWHM is approximately 3° in the case of SHG and of 7° for the fundamental beam. The latter value is consistent with the angular divergence of the fundamental beam outgoing the PhC. Besides, an additional SHG peak centered at $\varphi = 0^\circ$ is observed, which is absent in the linear indicatrix.

The SHG diffraction patterns measured when using the p- and s-polarized fundamental radiation and for $\theta = \theta_B$ presented in Fig. 2(b) show that an efficient SHG is observed only for the p polarization of the fundamental light, while the SHG indicatrix for the s-polarized fundamental radiation is absent within the experimental accuracy. We verified as well the absence of the SHG for the s-polarized fundamental beam. It is worth noting that despite the fact that the PhC is composed by an inhomogeneous nanoporous structure, the

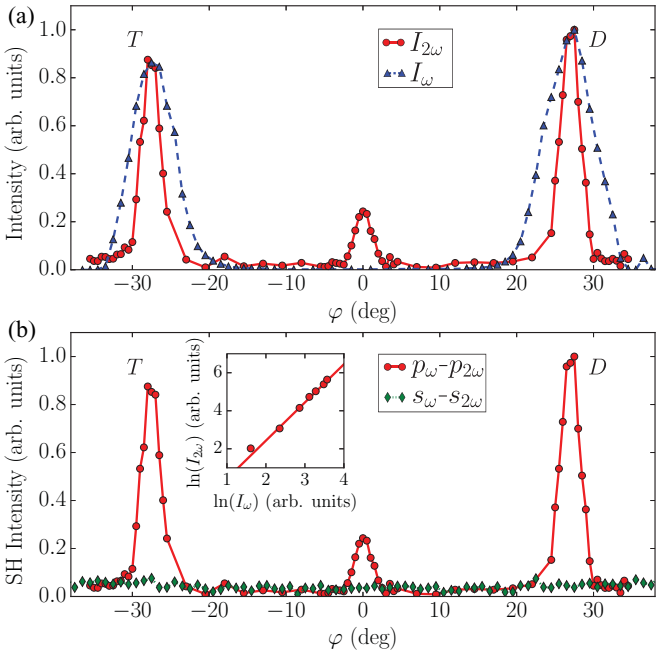

FIG. 2. (a) Fundamental (triangles, dashed blue line) and SHG intensity (circles, red line) diffraction patterns measured for $\theta_B = 27^\circ$. (b) SHG diffraction patterns measured when using the p-polarized (circles, red line) and s-polarized (rhombs, green line) fundamental radiation. T and D stand for the transmitted and diffracted beams directions.

SHG scattering turned out to be rather low as compared to the diffraction-induced SHG, as can be seen from Fig. 2(a). It appears as a wide SHG scattering indicatrix with the average amplitude being approximately two orders of magnitude smaller as compared to the SHG peak value in T or D maxima. A relatively small effect of the scattering processes in SHG for the studied samples is also supported by the estimations of the elastic scattering length that was made by a procedure discussed in Ref. [30]. Assuming spherical shape of pores in the PhC structure, it gives the characteristic scattering lengths for the fundamental wave of $l_\omega \sim 5$–13 mm and for the SH wave of $l_{2\omega} \sim 0.3$–0.8 mm. The relation $l_\omega \gg L$ proves that the scattering at the fundamental wavelength can be neglected, and the relation $l_{2\omega} \sim L$ indicates that while the scattering at the SH wave occurs, this process is not crucial and does not influence much the phase matched SHG.

We have also studied the SHG intensity as a function of the angle of incidence θ and of the diffraction angle φ, the corresponding pattern obtained for the p polarization of the fundamental beam is shown in Fig. 3. Here again the FWHM of the SHG maxima on the φ scale is less than 3.5° and the FWHM is only about 1.5° on the θ scale. In other words, as the angle of incidence is slightly detuned from the exact Bragg condition $\theta_B = 27^\circ$, the SHG intensity falls down rapidly. Again, a small intermediate SHG maximum centered at zero diffraction angle is observed, its angular width on the θ scale is also about 1.5°. In more detail, these properties of the SHG signal are discussed below when they are compared with the results of the theoretical description.

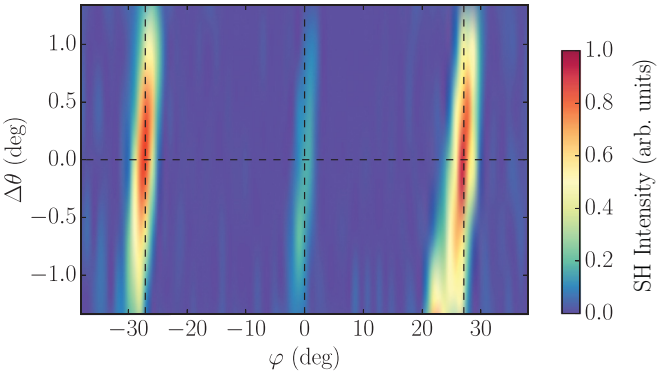

FIG. 3. SHG vs the angle of incidence $\Delta\theta = \theta - \theta_B$ and the diffraction angle φ; the color bar shows the SHG intensity in arb. units.

IV. MEASUREMENT OF REFRACTIVE INDEXES OF PHOTONIC CRYSTALS' LAYERS

To perform the further analysis, we need to estimate with a high accuracy the values of the refractive indexes of the layers, which form the PhC. This is a difficult task to get correct refractive index values of layers of 440 nm thick in the middle of the PhC structure when taking into account that the layers could become optically more inhomogeneous after the partial annealing.

To perform these measurements, we used the effect of diffraction-induced pulse splitting (DIPS), observed experimentally in Refs. [16,31] and which has not been exploited up to now as a diagnostics tool. The DIPS effect consists in a temporal splitting of the fundamental femtosecond laser pulse passed through a PhC in the Laue diffraction scheme into two pulses propagating with different group velocities. The splitting time is proportional to the product of the difference of the refractive indexes of the adjacent PhC layers and to the passing length inside a PhC [13,16]. The DIPS splitting time was shown to be on the subpicosecond range for a long enough PhC (hundreds of μm). It provides an accuracy of the determination of the refractive index of different PhC layers of at least 10^{-3}, which is a nontrivial task for an inhomogeneous (layered) structure. A more detailed procedure of refractive index determination is described in the Appendix. In our experiment, we made a series of measurements for different beam positions on the PhC facet. The mean values of n_1 and n_2 at 800 nm wavelength and their standard deviations are summarized in Table I.

As the determination of $n_{1,2}$ at the SHG wavelength of 400 nm by measuring the DIPS effect was technically impossible in our experiment, they were estimated by using the

TABLE I. Averaged values of the initial porosity and refractive indexes at the wavelengths of 800 nm and 400 nm for the two composing PhC layers.

Layer	ρ_{in},%	n_ω (800 nm)	$n_{2\omega}$ (400 nm)
1	65.0 ± 1.5	1.394 ± 0.005	1.415 ± 0.007
2	73.0 ± 1.5	1.316 ± 0.006	1.336 ± 0.009

Bruggeman model for the oxidized porous silicon films [32]. The effective refractive indexes of such a Si-SiO_2-air composite is a function $\varepsilon_{\text{eff}} = F(\rho_{\text{in}}, \varepsilon_{\text{Si}}, \varepsilon_{\text{SiO}_2}, \varepsilon_{\text{air}}, \beta)$, where ρ_{in} is the initial (before annealing) porosity of the Si-air composite, and ε_{Si}, $\varepsilon_{\text{SiO}_2}$, ε_{air} are dielectric susceptibilities of Si, SiO_2, and air, respectively. The annealing parameter β characterizes the ratio of the bulk fraction of the oxidized silicon to its initial content in a Si-air composite. The porosity of the layers was estimated from the reflection spectra measurement for the reference samples with the same structural parameters, the refractive indexes are estimated from the cross-correlation measurements at the wavelength 800 nm, and the $\varepsilon_{\text{Si}}, \varepsilon_{\text{SiO}_2}$ dependencies are known [33,34]. This allows us to calculate the refractive indexes of the two types of PhC layers at the SHG wavelength, $n_{2\omega}$. All the parameters of the PhC layers required for the further determination of the SHG phase matching conditions are summarized in Table I.

V. DISCUSSION

The theory of the nonlinear-optical interactions in 1D PhCs in the Laue diffraction scheme was first described by Mayer and Sukhorukov in Ref. [27]. It was predicted that the dynamical diffraction in the Laue geometry can result in the fulfillment of the phase-matching conditions for the SHG process involving different PhC eigenmodes, Borrmann or anti-Borrmann ones, at both the fundamental and SHG wavelengths. So the SHG phase-matching conditions take the form $\mathbf{q}^g(2\omega) = \mathbf{q}^i(\omega) + \mathbf{q}^j(\omega)$, where $g,i,j = \text{B},\text{aB}$. The vector diagram of the nonlinear process is shown in Fig. 1(b).

First, let us discuss possible mechanisms of SHG in porous silicon, which are responsible for the results discussed above. Crystalline silicon belongs to the crystallographic point symmetry group $m3m$, possesses the inversion symmetry, and thus the electric dipole second-order susceptibility is zero in the bulk of the crystal. At the same time, as was shown in previous works [35–37], the porous-silicon layers can be characterized by an *effective* dipole second-order susceptibility due to a large surface area of pores inside the structure. In our case, silicon was to a large extend oxidized to SiO_2, but residual silicon can produce surface-stress-induced and electric-field-induced second-order susceptibility on the interfaces between the layers with different porosity. The corresponding surface SH radiation can be generated if transversal component of the fundamental and SH fields are involved. Taking into account the experimental geometry shown in Fig. 1 this can be realized only for p-polarized fundamental and SH fields.

The SHG indicatrix measured for different angles of incidence θ (Fig. 3) shows that the SHG occurs in a narrow angular interval of about $\pm 0.75^\circ$ close to the Bragg angle. This indicates that SHG is synchronous, and the phase-matching conditions are fulfilled when the x projections of the Borrmann and anti-Borrmann wave vectors are equal to $h/2$ for the fundamental wave and to h for the SH one. The appearance of these two maxima that correspond to the T and D beams are attributed to the fulfillment of the phase-matching conditions discussed in Ref. [27]:

$$2\mathbf{q}(\omega) + l\mathbf{h} - \mathbf{q}(2\omega) = 0, \tag{1}$$

where $\mathbf{q}$ is the wave vector inside the PhC, $\mathbf{h}$ is the reciprocal lattice vector, $l = 0,2$.

We consider that the phase mismatch near the Bragg angle is determined predominantly by the z components of the wave vectors $\Delta q_z^{gij} = q_z^g(2\omega) - [q_z^i(\omega) + q_z^j(\omega)]$.

A. Analytical two-wave approach

Let us consider an analytical estimation for the fulfillment of the SHG phase-matching condition (1). In a particular case of the two-wave approximation, under the exact Bragg condition, and for a weak refraction index modulation $|n_1 - n_2| \ll n_0$ it gives the following expressions for the z projections of the wave vectors of the Borrmann and anti-Borrmann modes for the p-polarized fields [31]:

$$q_z^{\text{B,aB}}(\omega) = k\left(n_{\omega,0}^2 - \sin^2\theta_{\text{B}} \mp C_p|\epsilon_h|\right)^{1/2}, \tag{2}$$

where $n_{\omega,0} \approx (n_{\omega,1}d_1 + n_{\omega,2}d_2)/d$ is the average refractive index of the structure, $k = |\mathbf{k}| = 2\pi/\lambda$ is the wave number in vacuum, $C_p = 1 - 2n_{\omega,0}^{-2}\sin^2\theta_{\text{B}}$ is the polarization factor for the p-polarized fields, ϵ_h is the first Fourier component of the linear permittivity.

In the PhC sample used in our experiments the thicknesses of the layers are $d_1 = d_2$, and therefore the values of the second Fourier components are $\epsilon_{\pm 2h} = 0$. This means that in the two-wave approximation, the splitting of the dispersion curve for the SH radiation can be assumed to be negligibly small. Then the expression (2) for the SH field takes the simple form $q_z(2\omega) = 2k(n_{2\omega,0}^2 - \sin^2\theta_{\text{B}})^{1/2}$, where $n_{2\omega,0}$ is the averaged refractive index for the SH wave. The corresponding phase-matching condition (1) is performed accurately for the measured values $n_{1,2}$ within the error limits: $2q_z^{\text{aB}}(\omega) - q_z(2\omega) = 0$ for the $n_2(2\omega) = 1.3332$ and other indices are from the Table I.

B. Numerical calculation

In order to figure out the SHG phase-matching mechanism in PhC, the dispersion curves q_z vs the incident angle θ were calculated numerically using the revised plane-wave method (RPWM) [38]. In comparison to the two-wave approximation, RPWM method allows to take into account many waves propagating in a periodic medium. An intersection of the dispersion curves for the fundamental and SH waves indicates that the phase-matching conditions for the SHG process are fulfilled. The dispersion curves were calculated for the PhC studied in the experiment using the data summarized in Table I within the confidence interval of the refractive indexes variation, and thus the phase-matching conditions available in our PhC were estimated (1).

This is illustrated by Fig. 4, which shows the realization of three different types of the phase-matching conditions. The corresponding dependencies of the dispersion curves $q_{z,2\omega}^{\text{B,aB}}(\theta)$ for the Borrmann and anti-Borrmann modes at the SHG wavelength are shown in Figs. 4(a)–4(c) by green lines, while analogous dependencies for the fundamental wave are combined as a sum of various modes $q_{z,\omega}^i(\theta) + q_{z,\omega}^j(\theta)$ shown by red lines, θ is the angle of incidence.

Figure 4(a) demonstrates the SHG phase matching of the first type, attained for the two anti-Borrmann fundamental waves and also for the anti-Borrmann SHG mode (aB + aB →

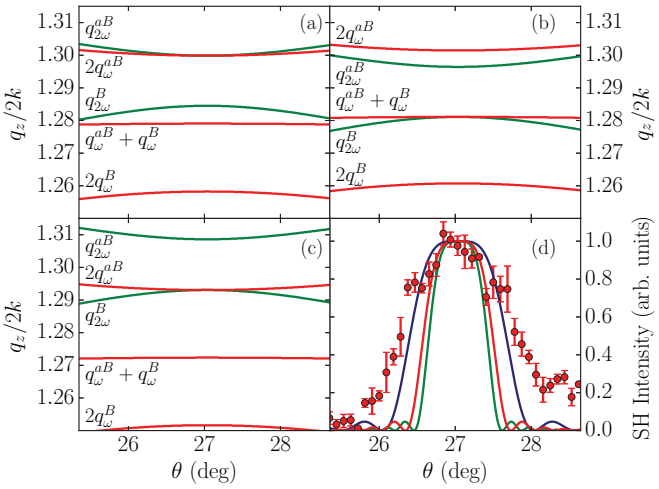

FIG. 4. Dispersion curves for three phase matching of type: (a) aB + aB → aB, (b) B + aB → B,(c) aB + aB → B; (d) angle distribution of SHG for three phase matchings of type (solid lines): aB + aB → aB (blue), B + aB → B (red), aB + aB → B (green). Calculated dependencies (d) were compared with experiment (points) for T direction. Calculation parameters were corresponded to parameters range of experimental PhC structure. For aB + aB → aB: $n_{1,\omega} = 1.397$, $n_{2,\omega} = 1.317$, $n_{1,2\omega} = 1.413$, $n_{2,2\omega} = 1.334$; for B + aB → B: $n_{1,\omega} = 1.398$, $n_{2,\omega} = 1.320$, $n_{1,2\omega} = 1.410$, $n_{2,2\omega} = 1.330$; for aB + aB → B: $n_{1,\omega} = 1.390, n_{2,\omega} = 1.311, n_{1,2\omega} = 1.421$, $n_{2,2\omega} = 1.342$.

aB). The second type of phase matching achieved when the Borrmann and anti-Borrmann fundamental waves generate the Borrmann-type SHG (B + aB → B) shown in Fig. 4(b). The third type of the phase-matching is obtained for two anti-Borrmann fundamental waves, which generate the Borrmann SHG (aB + aB → B) presented in Fig. 4(c). Only these three types of phase-matching conditions can be realized in the PhC under study. Figure 4(d) (filled circles) shows the experimental dependence of the SHG intensity on the angle of incidence θ close to the Bragg condition; it is a vertical cross section of Fig. 3. Solid lines represent numerical calculation of SHG intensity as a function of angle of incidence θ for the available phase-matching conditions.

C. Discussion of the experimental results: phase- and quasi-phase-matching SHG

The SHG indicatrices measured in the experiment (see Fig. 2) reveal the two narrow peaks in T and D directions with the width of about 3°. This is smaller than the width of the fundamental beams widths squared, which can be used as a reference in accordance with the simplest expression for the SHG intensity $I_{2\omega} \propto I_{\omega}^2$. Moreover, the corresponding theoretical estimate for the angular width of the SHG peaks is also small. This indicates that the phase-matched SHG takes place. The synchronous SHG in case of B + aB → B requires phase matching between the Borrmann and anti-Borrmann waves. However, in the case of short pump pulses the DIPS effect can be realized [31] due to different group velocities of the Borrmann and anti-Borrmann pulses, which split in time, therefore the B + aB → B phase matching can be realized only prior to

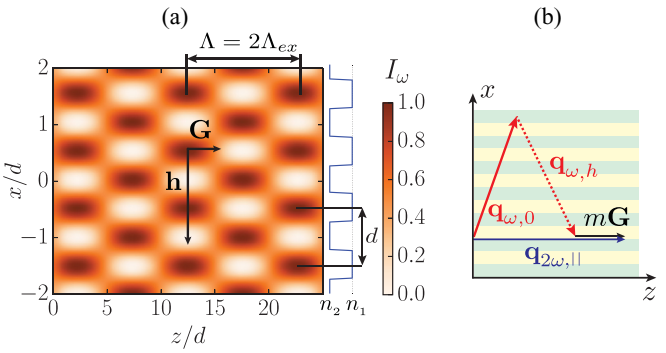

FIG. 5. (a) Fundamental intensity distribution by the interference of the Borrmann and anti-Borrmann modes under the dynamical diffraction at the Laue scheme. (b) Scheme of QPM for the SHG in the z direction with the wave vector $\mathbf{q}_{\|}(2\omega)$ using m induced reciprocal lattice vector $\mathbf{G}$.

the splitting of the Borrmann and anti-Borrmann pulses takes place. The quantitative parameter of the DIPS effect is the splitting length l_{DIPS}, which is the path passed by the pulses before the splitting time becomes equal to the doubled pulse duration. The pulse duration of the Ti:sapphire laser used in the SHG experiments was $\tau = 100$ fs. In this case, the splitting length $l_{\mathrm{DIPS}} \approx 1$ mm, which is two times larger as compared to the length of the sample. So the two pulses are coupled during the propagation inside the PhC, and synchronous SHG with phase-matching B + aB → B can take place.

Theoretical investigation in this paper and in Ref. [27] were made for continuous waves, while in the experiment short pulses with $\Delta\lambda_{\mathrm{FWHM}} \approx 10$ nm of a Ti:sapphire laser were used. The influence of a finite spectra of the fundamental wave leads also to broadening of the angular SHG peaks in comparison to the calculated ones, which is proved by the experimental results presented in Fig. 4(d).

The appearance of the SHG maximum centered at $\varphi = 0$ (see Fig. 2) can be explained by the existence of an electric-field-induced lattice of the effective second-order susceptibility $\chi^{(2)}(x,z)$ induced in porous-silicon structure by the p-polarized fundamental radiation. The origin of the nonlinear lattice is the spatial periodic structure of the fundamental field formed by the interference of the Borrmann and anti-Borrmann modes under the dynamical diffraction at the Laue scheme, i.e., the so-called pendulum effect [17–20].

The mechanism of the effect is illustrated by Fig. 5(a), which shows that the spatial structure of the intensity $I_\omega(x,z)$ in porous silicon in this case has a rectangular centered lattice with the periods d transverse to the z axis and $\Lambda = 2\Lambda_{\mathrm{ex}} = \lambda(n_{\omega,0}^2 - \sin^2\theta_{\mathrm{B}})^{1/2}/C^{(p)}|\epsilon_h|$ along the z axis. Here Λ is the period of pendulum effect, or the period of the total transfer of energy from the transmitted to the diffracted waves and vice versa, and Λ_{ex} is the extinction depth [14]. In the regions of the maximal intensity $I_\omega(x,z)$ the internal photoemission of electrons from silicon, and their subsequent capturing in surface traps of thin SiO_2 layer takes place. Thus a spatially modulated charge distribution appears in the interfacial Si/SiO_2 region, which results in the formation of periodically modulated quasi-static interfacial electric field E_{DC} [39,40]. In turn, this electric field leads

to the emergence of the electric-field-induced second-order susceptibility $\chi^{(2)}(x,z) = 3\chi^{(3)}E_{DC}(x,z)$, where $\chi^{(3)}$ is cubic susceptibility of Si-SiO_2 interface region.

This mechanism provides an additional SH source in Si-SiO_2 PhC. The nonlinear lattice of $\chi^{(2)}(x,z)$ has the same spatial distribution as the pump intensity $I_\omega(x,z)$ and adds a new reciprocal lattice vector $\mathbf{G} = (2\pi/\Lambda)\mathbf{e}_z$ in QPM condition (3), where $\mathbf{e}_z$ is the unit vector along the axis z. This leads to a new quasi-phase-matching (QPM) condition, which involves this additional $\mathbf{G}$ vector [2,4]:

$$\mathbf{q}(\omega) + \mathbf{q}(\omega) + m\mathbf{G} + l\mathbf{h} - \mathbf{q}(2\omega) = 0, \tag{3}$$

where $m,l = 0, \pm 1, \ldots$ are the orders of QPM.

Figure 5(b) shows the scheme of QPM for the SHG for a wave propagating along the layers of the structure in the z direction with the wave vector $\mathbf{q}_\parallel(2\omega)$, which is far away from the diffraction Bragg condition:

$$\mathbf{q}_0(\omega) + (\mathbf{q}_0(\omega) + \mathbf{h}) + m\mathbf{G} - \mathbf{q}_\parallel(2\omega) = 0, \tag{4}$$

where $\mathbf{q}_\parallel(2\omega)=2kn_{2\omega,0}\mathbf{e}_z$ and $\mathbf{q}_0(\omega)$ is the wave vector of the transmitted fundamental field. For the experimental parameters considered above, the condition (4) is fulfilled for the anti-Borrmann mode in the fourth order of QPM: $2q_z^{aB} - q_\parallel(2\omega) + 4G = 0$. It is easy to show from Eq. (2) that since the difference between the wave vector's projections is $q_z^{aB}(\omega) - q_z^{B}(\omega) = G$, the QPM of higher orders $m = 5,6$ are satisfied also for other waves combinations: $q_z^{B}(\omega) + q_z^{aB}(\omega) - q_{||}(2\omega) + 5G = 0$ and $2q_z^{B}(\omega) - q_{||}(2\omega) + 6G = 0$.

So the central SH maximum in Fig. 2 can be explained by QPM SHG in originally centrosymmetric PhC due to the second-order susceptibility lattice induced by the electric field of the space charge at the Si/SiO_2 interface in the presence of the diffraction pendulum effect.

VI. CONCLUSIONS

Summing up, we have studied experimentally optical SHG in 1D porous-silicon-based PhCs in the Laue diffraction scheme. By analyzing the angular and spectral width of the SHG diffraction maxima we confirm the phase-matched second-harmonic generation process. Numerical analysis of the dispersion curves of the studied PhC shows that the phase-matching conditions can be realized when exciting the SHG by the Borrmann and anti-Borrmann modes in our experimental conditions. An additional type of SHG synchronism attributed to electric-field-induced lattice of second-order susceptibility in Si/SiO_2-based PhC is suggested.

ACKNOWLEDGMENT

This work was partially supported by the Russian Foundation for Basic Research Grants No. 16-02-01100 and No. 14-29-07197.

APPENDIX: MEASUREMENT OF REFRACTIVE INDEXES OF PHOTONIC CRYSTALS' LAYERS BY THE DIPS EFFECT

In DIPS experiments, a cross-correlation (CC) technique was used to determine the time delay of the split pulses leaving the PhC. Linearly polarized radiation of a 30 fs Ti:sapphire laser operating at 800 nm wavelength served as a source of the fundamental radiation and a CC scheme with the signal (S) and the reference (R) arms containing prism compressors was used. We measured the cross-correlation function at the fundamental frequency as $I_{CC}(\tau) \propto \int_{-\infty}^{\infty} I_S(t)I_R(t+\tau)dt$, where $I_S(t)$ and $I_R(t+\tau)$ are the intensities measured in the signal and reference channels of the setup, and τ is the delay time between them.

The experimental procedure for the determination of the refractive indices n_1 and n_2 was as follows. First, the I_{CC} function without the PhC was measured, so the time T_0 of a single laser pulse passing the optical distance between the laser source and the detector inside the set-up, $L_0 = cT_0$, was estimated, where c is speed of light. Second, I_{CC} was measured after the PhC set at $\theta = \theta_B$ was introduced in the setup. The two laser pulses outgoing the PhC were observed, coming at the times T^B (Borrmann pulse) and T^{aB} (anti-Borrmann pulse): $T^{B,aB} = (L_0 - L_{PhC})/c + L_{PhC}/v_{exp}^{B,aB}$, where L_{PhC} is the PhC length. In turn, this allows for the calculation of the experimental value of Borrmann and anti-Borrmann group velocity $v_{exp}^{B,aB}$.

An analytical expression for the group velocities $v_g^{B,aB}$ under the Bragg diffraction conditions was obtained in the two-wave approach in Ref. [31], which revealed the dependence of $v_g^{B,aB}$ on the PhC parameters $n_{1,2}$,$d_{1,2}$. This gives a system of the two equation for $v_g^{B}(n_1,n_2)$ and $v_g^{aB}(n_1,n_2)$:

$$\begin{aligned} c\frac{q_z^{B}}{k}\left[\epsilon_0 - \frac{C_j\epsilon_h\epsilon_{-h}k^2(2C_j + \omega\partial C_j/\partial\omega)}{2\sqrt{h^2\alpha_0^2 + C_j^2\epsilon_h\epsilon_{-h}k^4}}\right]^{-1} &= v_{exp}^{B}, \\ c\frac{q_z^{aB}}{k}\left[\epsilon_0 + \frac{C_j\epsilon_h\epsilon_{-h}k^2(2C_j + \omega\partial C_j/\partial\omega)}{2\sqrt{h^2\alpha_0^2 + C_j^2\epsilon_h\epsilon_{-h}k^4}}\right]^{-1} &= v_{exp}^{aB}, \end{aligned} \tag{A1}$$

where $k = |\mathbf{k}| = \omega/c$ is the wave number in vacuum, $q_z^{B,aB} = k^2\epsilon_0 - q_{0x}^2 + h\alpha_0 \mp \sqrt{h^2\alpha_0 + C_j^2\epsilon_h\epsilon_{-h}k^4}$ are the z projection and $q_{0x} = k\sin\theta_B$ is the x projection of the Borrmann and anti-Borrmann wave vectors, $\alpha_0 = q_{0x} - h/2$, ϵ_0, ϵ_h, ϵ_{-h} are the Fourier components of the permittivity, C_j are the polarization factors for the p- and s-polarized field [31]. Taking into account the dependencies of ϵ_0, ϵ_h, ϵ_{-h}, $q_z^{B,aB}$, C_j on n_1 and n_2, the numerical solution of the system (A1) gives the values of the *true* refractive indexes of the PhC layers n_1 and n_2. It is worth noting that the dependencies $v_g^{B}(n_1,n_2)$ and $v_g^{aB}(n_1,n_2)$ can be obtained as well by numerical methods as in Ref. [38].

[1] J. A. Armstrong, N. Bloembergen, J. Ducuing, and P. S. Pershan, Phys. Rev. **127**, 1918 (1962).

[2] M. M. Fejer, G. A. Magel, D. H. Jundt, and R. L. Byer, IEEE J. Quantum Electron. **28**, 2631 (1992).

[3] D. Faccio, F. Bragheri, and M. Cherchi, J. Opt. Soc. Am. B **21**, 296 (2004).
[4] V. Berger, Phys. Rev. Lett. **81**, 4136 (1998).
[5] N. G. R. Broderick, G. W. Ross, H. L. Offerhaus, D. J. Richardson, and D. C. Hanna, Phys. Rev. Lett. **84**, 4345 (2000).
[6] A. Yariv and P. Yeh, J. Opt. Soc. Am. **67**, 438 (1977).
[7] J. Martorell, R. Vilaseca, and R. Corbalan, Phys. Rev. A **55**, 4520 (1997).
[8] M. Centini, C. Sibilia, M. Scalora, G. D'Aguanno, M. Bertolotti, M. J. Bloemer, C. M. Bowden, and I. Nefedov, Phys. Rev. E **60**, 4891 (1999).
[9] A. V. Balakin, V. A. Bushuev, B. I. Mantsyzov, I. A. Ozheredov, E. V. Petrov, A. P. Shkurinov, P. Masselin, and G. Mouret, Phys. Rev. E **63**, 046609 (2001).
[10] T. Baba, Nat. Photon. **2**, 465 (2008).
[11] P. St.J. Russell, Phys. Rev. Lett. **56**, 596 (1986).
[12] B. I. Mantsyzov, Opt. Commun. **189**, 275 (2001).
[13] V. A. Bushuev, B. I. Mantsyzov, and A. A. Skorynin, Phys. Rev. A **79**, 053811 (2009).
[14] A. A. Skorynin, V. A. Bushuev, and B. I. Mantsyzov, J. Exp. Theor. Phys. **115**, 56 (2012).
[15] X. Yan, L. Gao, Y. Dai, X. Yang, Y. Chen, and G. Ma, Opt. Express **22**, 18527 (2014).
[16] S. E. Svyakhovskiy, V. O. Kompanets, A. I. Maydykovskiy, T. V. Murzina, S. V. Chekalin, A. A. Skorynin, V. A. Bushuev, and B. I. Mantsyzov, Phys. Rev. A **86**, 013843 (2012).
[17] M. L. Calvo, P. Cheben, O. Martinez-Matos, F. del Monte, and J. A. Rodrigo, Phys. Rev. Lett. **97**, 084801 (2006).
[18] A. Balestreri, L. C. Andreani, and M. Agio, Phys. Rev. E **74**, 036603 (2006).
[19] S. Savo, E. Di Gennaro, C. Miletto, A. Andreone, P. Dardano, L. Moretti, and V. Mocella, Opt. Express **16**, 9097 (2008).
[20] V. B. Novikov, S. E. Svyakhovskiy, A. I. Maydykovskiy, T. V. Murzina, and B. I. Mantsyzov, J. Appl. Phys. **118**, 193101 (2015).
[21] S. E. Svyakhovskiy, A. A. Skorynin, V. A. Bushuev, S. V. Chekalin, V. O. Kompanets, A. I. Maydykovskiy, T. V. Murzina, and B. I. Mantsyzov, Opt. Express **22**, 31002 (2014).
[22] S. E. Svyakhovskiy, A. I. Maydykovsky, and T. V. Murzina, J. Appl. Phys. **112**, 013106 (2012).
[23] M. Cavanagh, J. R. Power, J. F. McGilp, H. Munder, and M. G. Berger, Thin Solid Films **255**, 146 (1995).
[24] M. Falasconi, L. C. Andreani, A. M. Malvezzi, M. Patrini, V. Mulloni, and L. Pavesi, Surf. Sci. **481**, 105 (2001).
[25] L. A. Golovan, V. Yu. Timoshenko, A. B. Fedotov, L. P. Kuznetsova, D. A. Sidorov-Biryukov, P. K. Kashkarov, A. M. Zheltikov, D. Kovalev, N. Knzner, E. Gross, J. Diener, G. Polisski, and F. Koch, Appl. Phys. B **73**, 31 (2001).
[26] T. V. Murzina, I. A. Kolmychek, A. I. Maidykovski, A. A. Nikulin, F. Yu. Sychev, and O. A. Aktsipetrov, Opt. Lett. **33**, 2581 (2008).
[27] A. A. Maier and A. P. Sukhorukov, Sov. Phys. JETP **50**, 4 (1979).
[28] A. Nazarkin, S. Podorov, I. Uschmann, E. Forster, and R. Sauerbrey, Phys. Rev. A **67**, 041804(R) (2003).
[29] S. Shwartz, M. Fuchs, J. B. Hastings, Y. Inubushi, T. Ishikawa, T. Katayama, D. A. Reis, T. Sato, K. Tono, M. Yabashi, S. Yudovich, and S. E. Harris, Phys. Rev. Lett. **112**, 163901 (2014).
[30] V. E. Kravtsov, V. M. Agranovich, and K. I. Grigorishin, Phys. Rev. B **44**, 4931 (1991).
[31] S. E. Svyakhovskiy, A. A. Skorynin, V. A. Bushuev, S. V. Chekalin, V. O. Kompanets, A. I. Maydykovskiy, T. V. Murzina, V. B. Novikov, and B. I. Mantsyzov, J. Opt. Soc. Am. B **30**, 1261 (2013).
[32] E. Astrova and V. Tolmachev, Mater. Sci. Eng. B **69–70**, 142 (2000).
[33] D. E. Aspnes and A. A. Studna, Phys. Rev. B **27**, 985 (1983).
[34] L. Gao, F. Lemarchand, and M. Lequime, J. Europ. Opt. Soc. Rap. Public. **8**, 13010 (2013).
[35] A. I. Maidykovski, N. M. Nagorskii, T. V. Murzina, A. A. Nikulin, S. A. Magnitskii, and O. A. Aktsipetrov, JETP Lett. **94**, 451 (2011).
[36] T. V. Dolgova, A. I. Maidykovski, M. G. Martemyanov, A. A. Fedyanin, O. A. Aktsipetrov, G. Marowsky, V. A. Yakovlev, G. Mattei, N. Ohta, and S. Nakabayashi, J. Opt. Soc. Am. B **19**, 2129 (2002).
[37] L. A. Golovan and V. Yu. Timoshenko, J. Nanoelectron. Optoelectron. **8**, 223 (2013).
[38] Sh. Shi, C. Chen, and D. W. Prather, Appl. Phys. Lett. **86**, 043104 (2005).
[39] J. Bloch, J. G. Mihaychuk, and H. M. van Driel, Phys. Rev. Lett. **77**, 920 (1996).
[40] Z. Marka, R. Pasternak, S. N. Rashkeev, Y. Jiang, S. T. Pantelides, N. H. Tolk, P. K. Roy, and J. Kozub, Phys. Rev. B **67**, 045302 (2003).